

# Analysis of coseismic surface displacement gradients using radar interferometry: New insights into the Landers earthquake

Gilles Peltzer

Jet Propulsion Laboratory, California Institute of Technology, Pasadena

Kenneth W. Hudnut

U.S. Geological Survey, Pasadena, California

Kurt L. Feigl

Centre National de la Recherche Scientifique, Observatoire Midi-Pyrénées, Toulouse, France

**Abstract.** The map of the coseismic displacement field generated by interferometric processing of synthetic aperture radar (SAR) images taken before and after the June 28, 1992, Landers earthquake sequence brings new insights into the nature of deformation caused by these earthquakes. We use the interferometric map generated by Massonnet et al. (1993) to analyze the surface displacement field in the vicinity of the fault trace. Complexities in the fringe pattern near the fault reflect short-wavelength variations of the surface rupture and slip distribution, and attest to large displacement gradients. Along two sections of the fault, characteristic fringe patterns can be recognized, contrasting in density and direction with patterns observed away from the rupture. In order to understand the observed fringe patterns, we compute synthetic interferograms in three simple cases: (1) rigid-body rotations about a vertical axis, (2) about a horizontal axis (tilt), and (3) distributed, simple shear. The orientation and spatial separation of interferometric fringes predicted by these models help constrain near-field deformation and rupture parameters. Where the Kickapoo fault connects with the Homestead Valley fault, the interferogram shows a clear pattern of parallel N20°W fringes separated by about 160 m. This pattern and vertical offsets measured along the Kickapoo fault suggest that the block between this fault and the Johnson Valley fault may have been tilted, down to the west. A 5-km block lifted by 1 m on one side would be tilted by an angle of 0.01° (190  $\mu$ rad), producing fringes separated by about 160 m, parallel to the tilt axis. Such a tilt, parallel to a N20°W direction, would account for the gradual, northward increase of the vertical slip component observed along the Kickapoo fault. This tilt may also explain the 1 m of reverse slip observed along the "slip gap" section of the Homestead Valley break. Between the southern end of the Johnson Valley fault and the Eureka Peak fault, where no surface rupture has been mapped, the dense pattern of fringes implies distributed shear, probably resulting from fault slip at depth. The density and direction of the fringes in the gap are consistent with a right-lateral slip of 1.2-3.8 m on a blind fault locked above the depth of 1.5-2 km. Such observations of small wavelength features in the SAR interferogram bring new insights into the near-field displacement gradient and thus on response of the uppermost crust to seismic rupture.

## Introduction

The June 28, 1992, Landers, California,  $M=7.5$  earthquake provided the first opportunity to apply the technique of synthetic aperture radar (SAR) interferometry to detect coseismic ground displacement [Massonnet et al., 1993; Zebker et al., 1994b]. The interferogram produced by differencing the phase between two SAR images taken before and after the earthquake provides a contour map of the component of the surface displacement field parallel to the

vector between the ground point and the satellite. The relation between a particular fringe pattern observed in an interferogram and the actual displacement field of the ground is not straightforward. Since the radar depicts only one component of the displacement field, resolving the three components of the surface displacement vector requires independent observations and reliance on modeling.

For the Landers earthquake, a simple elastic dislocation model, based on the rupture map and surface offset measurements at the fault, appears to account for most of the fringes observed in the far and intermediate fields [Massonnet et al., 1993]. In most places, the difference between the observed and predicted range displacement is less than two cycles (the wavelength of the ERS-1 C band radar is 56.6 mm). Within 5 km of the faults, however, the rupture pattern

Copyright 1994 by the American Geophysical Union.

Paper number 94JB01888.  
0148-0227/94/94JB-01888\$05.00

involved extensive secondary faulting, overlapping segments, and numerous fissures, resulting in a complex displacement field depicted by dense fringe patterns and zones of incoherence in the interferogram (Figure 1) which are not accounted for by the simple elastic model described by *Massonnet et al.* [1993]. In an attempt to understand the small-scale features of the Landers earthquake interferogram in the vicinity of the fault breaks, we compute synthetic interferograms for simple examples of displacement fields that one may expect near a fault surface rupture. We then compare these synthetic interferograms with the fringe patterns observed in the interferogram published by *Massonnet et al.* [1993] at two selected areas along the fault. These areas include (1) the northern end of the Johnson Valley fault, where it merges with the Kickapoo fault, and (2) the surface rupture gap between the southern end of the Johnson Valley fault and

the Eureka Peak fault (Figure 1). For these two sites, we confront the inferences based on the radar interferogram with field observations and results of inversion of geodetic data.

### Examples of Simple Fringe Pattern

In order to understand the complexity of the patterns observed in the interferogram in the vicinity of the rupture, we compute synthetic interferograms produced in three simple cases: (1) rigid-body rotation about a vertical axis, (2) about a horizontal axis (tilt), and (3) distributed simple shear. For each of these three cases, we compute the slant-range component (parallel to the satellite line of sight) of the ground displacement vectors, and derive the orientation of the resulting fringes and their spatial separation. In an Earth fixed reference frame, the satellite line of sight lies in the plane

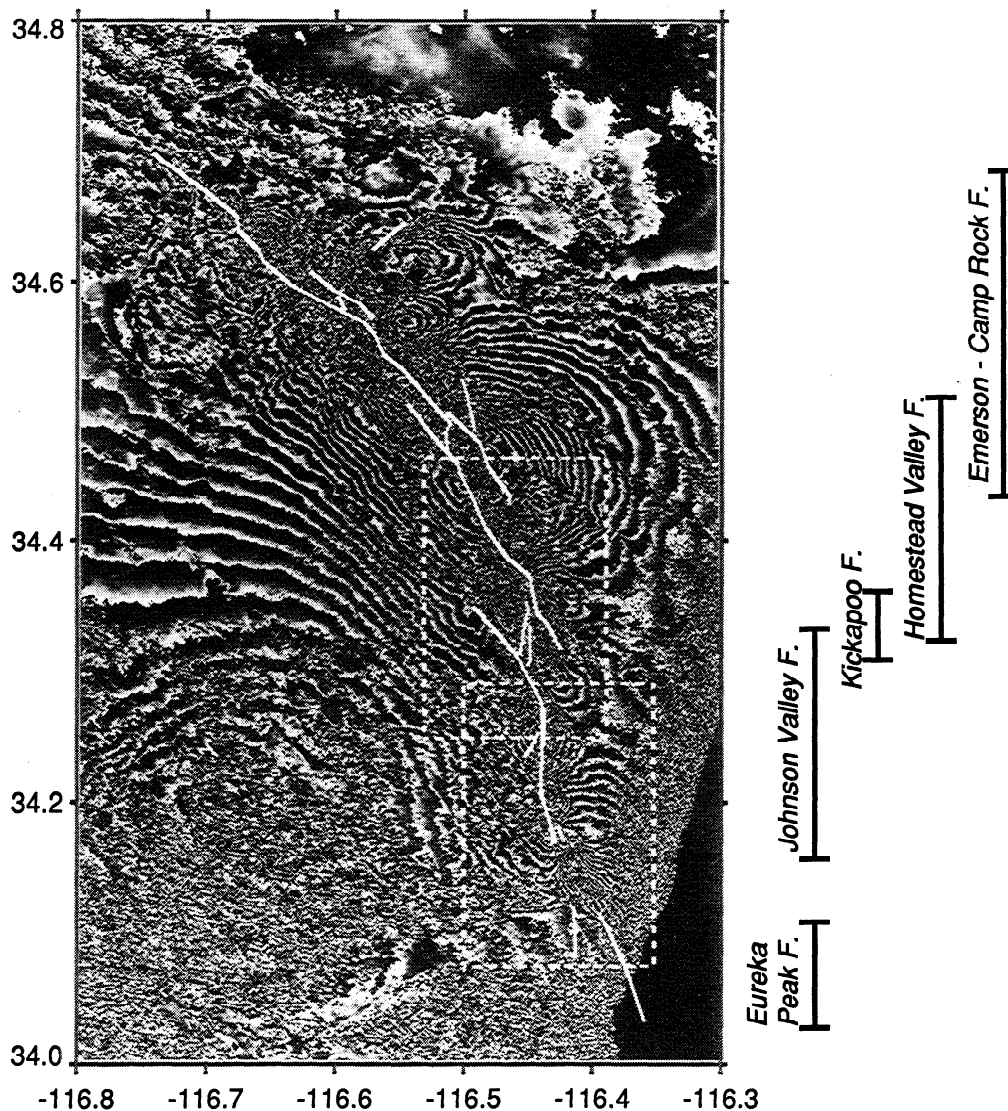


**Figure 1.** Coseismic interferogram of the Landers, June 28, 1992 earthquake obtained with ERS-1 SAR data [*Massonnet et al.*, 1993]. Fringes are contour lines of equal displacement of the ground along the line of sight of satellite. One full gray-scale cycle represents 2.83 cm of surface displacement parallel to the line of sight. Surface rupture, shown in white, is simplified from *Hart et al.* [1993]. Dashed boxes delineate areas of fringe patterns investigated in this paper.

containing the satellite and the perpendicular to the satellite track. Therefore, the slant-range component of a horizontal displacement vector is the projection of that vector onto the satellite cross-track direction multiplied by the sine of the incidence angle (the angle between the satellite line of sight and the local vertical direction, Figure 2). Similarly, the range component of a vertical displacement vector is the magnitude of that vector multiplied by the cosine of the incidence angle (Figure 2).

The domains in which such simple deformation figures occur are unlikely to extend more than 2 to 5 km across the SAR image width, i.e., approximately the distance between overlapping branches of the fault. Hence we assume that the incidence angle of the radar beam remains constant across the area involved. Since the near- and far-range incidence angles for ERS-1 SAR images are 20.1° and 25.9°, respectively [European Space Agency, 1992], we use the average value of 23°.

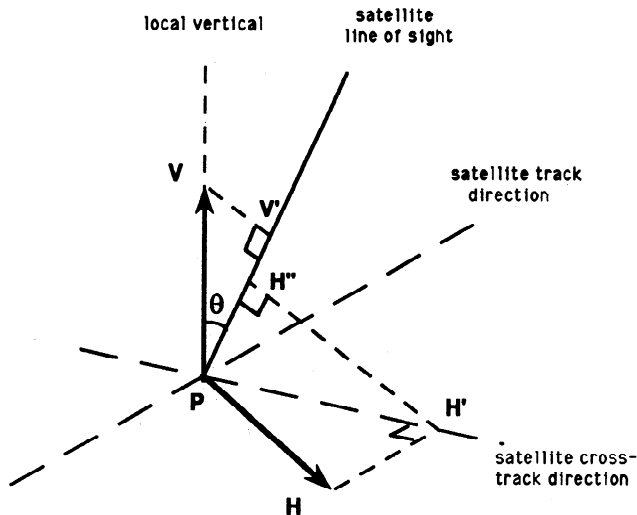
**Block Rotation and Tilt**

Figure 3a shows the case of a rigid-body rotation of a crustal block about a vertical axis. The projection of the incremental displacement vector onto the cross-track direction remains constant along straight lines parallel to that direction. Therefore fringes, which are lines of equal displacement in the range direction, are straight lines trending perpendicular to the satellite track direction. For a small rotation angle  $r$ , the distance between consecutive fringes is given by

$$d_r = \lambda / [2r \sin(\theta)], \tag{1}$$

where  $\lambda$  is the radar wavelength (56.6 mm) and  $\theta$  is the incidence angle (23°).

Figure 3b shows the case of a tilted crustal block, i.e., a rigid-body rotation about a horizontal axis. For a small rotation angle  $t$ , the displacement vectors of ground points are essentially vertical and remain constant along straight lines parallel to the tilt axis. The fringes are thus parallel to the tilt



**Figure 2.** Sketch showing projections PH'' and PV' of horizontal (PH) and vertical (PV) vectors on the satellite line of site, respectively;  $\theta$  is the incidence angle.

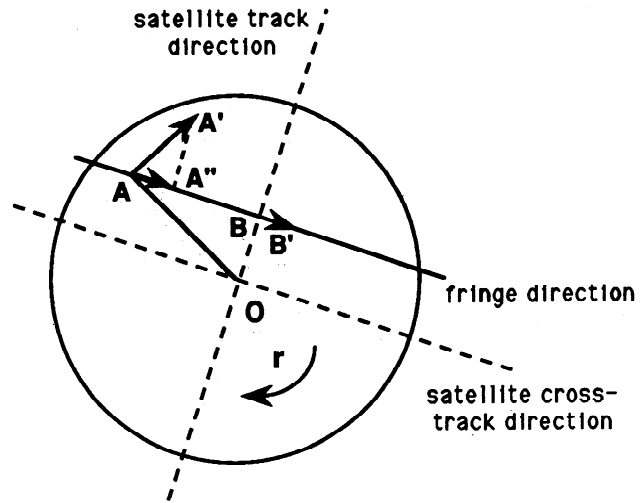


**Figure 3a.** Sketch in map view showing geometry of displacement vector in the case of rigid-body rotation about a vertical axis. Projection AA'' of displacement vector AA' onto satellite cross-track direction AB is constant along that direction. Fringes are thus parallel to that direction, i.e., perpendicular to satellite track direction.

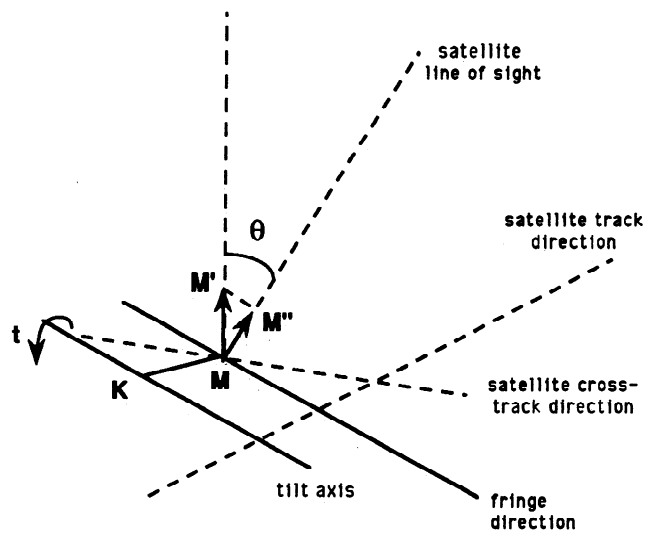


**Figure 3b.** Sketch in perspective view showing displacement vector in the case of rigid-body rotation about a horizontal axis (tilt).  $\theta$  is the satellite incidence angle. For small rotation angle  $t$ , displacement vector MM' is vertical and proportional to distance MK to tilt axis. Vector MM' and projection MM'' onto satellite line of sight is constant along lines parallel to tilt axis. Fringes are thus parallel to tilt axis.

axis, and the interval between consecutive fringes is given by

$$d_t = \lambda / [2t \cos(\theta)]. \tag{2}$$

Synthetic interferograms corresponding to the two rotation cases above and for various angles of rotation are shown in Figure 4a. Figure 4b depicts the variation of distances  $d_r$  and  $d_t$  with rotation angles  $r$  and  $t$ , respectively. For a rotation angle of about 0.2° and a tilt angle of about 0.1°, the distance between fringes is of the same order of magnitude as the

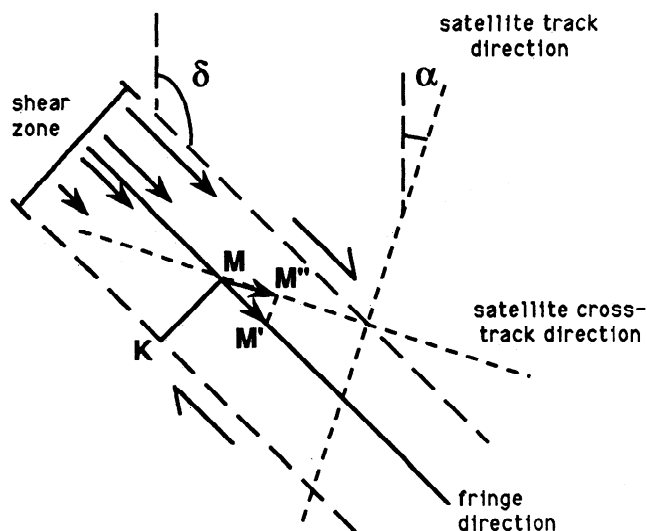


**Figure 3c.** Sketch in map view showing displacement vector in the case of simple, distributed shear. Displacement vector  $MM'$  is proportional to distance  $KM$  to edge of shear zone. Projection  $MM''$  of  $MM'$  onto cross-track direction is constant along lines parallel to the shear direction. Fringes are thus parallel to the shear direction.  $\delta$  is the shear direction azimuth, and  $\alpha$ , the satellite track azimuth.

ground pixel spacing in the SAR image, assuming relatively flat terrain (20 m in ground range for the ERS-1 SAR). This means that for angles greater than these values the interferogram becomes incoherent because the phase variation across each pixel exceeds one cycle.

*Zebker and Villasenor* [1992] have studied the decorrelation of interferometric radar echoes resulting from change in the apparent distributions of scatterers within each image pixel. Their results show in particular that *C* band (56.6 mm) radar echoes of two images decorrelate completely if the ground rotates about  $0.7^\circ$  with respect to the satellite line of sight between the two images. The limiting value of  $0.2^\circ$  noted above for horizontal rotations, which depends on the size of the ERS-1 SAR image pixel, is reached before signal decorrelation occurs in the sense of *Zebker and Villasenor* [1992]. For the interferogram of the Landers earthquake, the SAR image has been averaged over 90-m pixels in order to be combined with the USGS digital elevation model used to remove the topographic signal [*Massonnet et al.*, 1993] (Figure 1). For such a pixel size, the fringes produced by block rotations or tilts become invisible for rotation angles of approximately  $0.04^\circ$  and  $0.02^\circ$ , respectively (Nyquist effect, Figure 4b).

### Distributed Shear

In a shear zone where simple shear is evenly distributed across a zone of finite width, the displacement of a ground point is proportional to the distance between the point and the edge of the shear zone (Figure 3c). The displacement vectors remain constant along straight lines parallel to the shear direction, and the resulting fringes are thus parallel to that direction. The distance between consecutive fringes is given by

$$d_s = \lambda / [2\gamma \sin(\delta - \alpha) \sin(\theta)], \quad (3)$$

where  $\alpha$  is the satellite track azimuth,  $\delta$ , the shear zone

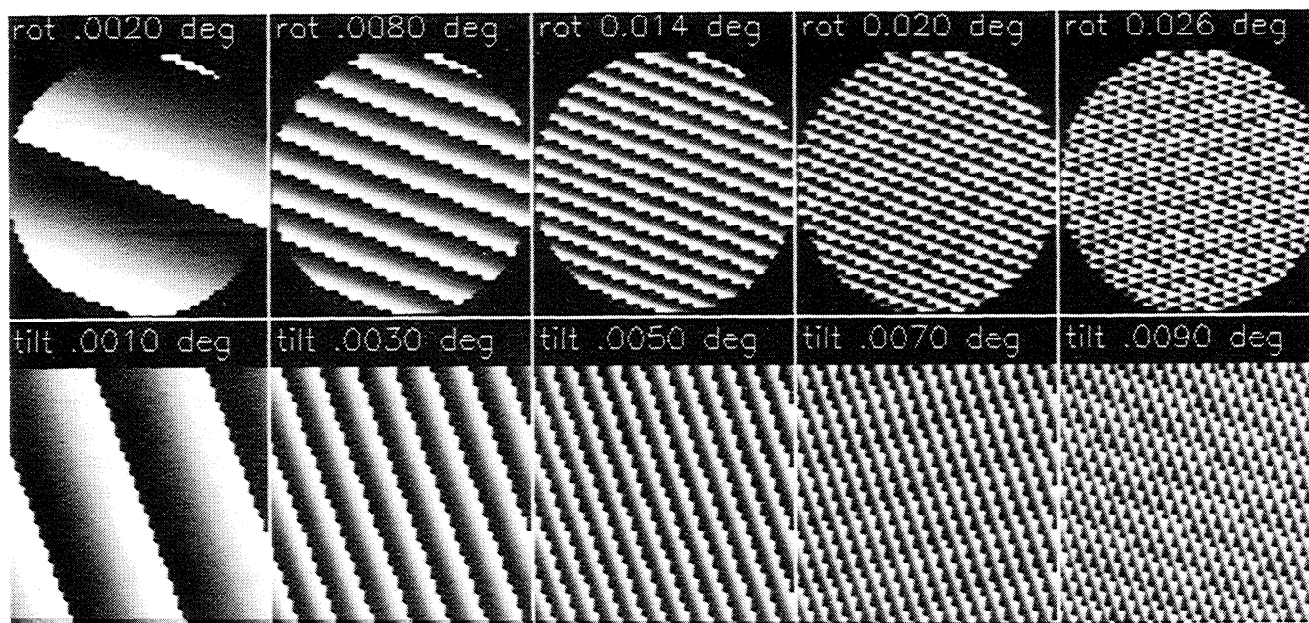


**Figure 4a.** Synthetic interferograms generated in the case of rigid-body rotations about a vertical axis (upper row) and tilts (lower row) for five different rotation angles. Rotation angles are indicated in degrees. Size of boxes represents 5 km on the ground on a flat terrain. Small steps in fringes are image pixels assumed to be 90 m, as for interferogram of Figure 1. Fringes are perpendicular to satellite track direction ( $N20^\circ E$  in example shown) for rotations about vertical axis and parallel to rotation axis ( $N160^\circ E$  in example shown) for tilts.

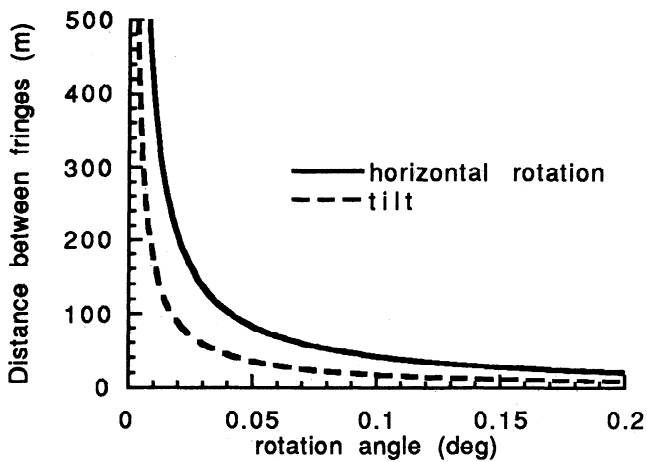


**Figure 4b.** Curves showing decrease of fringe separation with increasing rotation angle in cases of Figure 4a.

azimuth and  $\gamma$ , the shear coefficient (Figure 3c). Note that for shear zones striking in the direction of the satellite track ( $\delta=\alpha$ ), this distance is not defined. This is due to the fact that any displacement of the ground in the direction of the satellite track has a null projection onto the range axis. Therefore, a distributed shear zone parallel to the satellite track would not produce any fringes in an interferogram.

### Quantitative Analysis of the Displacement Gradient in the Vicinity of the Rupture

A combination of the simple cases considered above would result in complex fringe patterns which may be difficult to predict and interpret uniquely. However, the information provided by the interferogram may be combined with independent field observations of the geometry of the rupture and offset distribution to constrain models of a seismic event. In this section, we analyze the coseismic displacement field in the vicinity of the Landers earthquake rupture zone and examine in detail two segments of the fault where dense fringe patterns are observed.

One of the most striking features apparent in the Landers earthquake coseismic interferogram is the narrow band with no coherent fringes along most of the fault (Figure 1). Such a feature indicates very low correlation between the two images used to build the interferogram. Although many changes due to the violent ground motion may have affected the ground surface during the earthquake, the most likely reason for such a decorrelation is the increase of the displacement gradient in the vicinity of the rupture [Zebker and Villasenor, 1992; Massonnet et al., 1993; Zebker et al., 1994b]. High displacement gradients produce dense interferometric fringe patterns which cannot be depicted in a digital image when the distance between the fringes becomes smaller than the size of the image pixel. In our study, the limiting threshold is the 90-m pixel size of the averaged radar image. Using the full-resolution SAR images would help to analyze regions of high strain provided that the data noise is sufficiently low [e.g., Goldstein et al., 1993]. In some areas along the fault where detailed mapping has been done, numerous secondary faulting

and fissures are reported, attesting to high strain within the volume of crust adjacent to the main surface break [e.g., Sieh et al., 1993; Johnson et al., 1993; Hart et al., 1993; Sowers et al., 1994]. Studying the deformation field in such areas is beyond the present capability of the interferometric technique, given the resolution of the ERS-1 SAR data.

### The Johnson Valley Fault - Kickapoo Fault Junction

The Kickapoo fault (also called the Landers fault [Sieh et al., 1993]) crosses from the northern Johnson Valley fault towards the southern Homestead Valley fault, where these two faults overlap over a distance of 6 km (Figure 5). The distribution of coseismic lateral displacement along these three faults shows that the Kickapoo fault progressively transfers the 3-4 m of right lateral slip from the Johnson Valley fault to the Homestead Valley fault [Sowers et al., 1994]. North of the Kickapoo fault, the Southern Homestead Valley fault extends for about 1 km in a north-south direction, and the mostly right-lateral slip on the fault abruptly drops to zero [Sieh et al., 1993; Spotila and Sieh, 1994]. The surface break reappears ~500 m farther north along a more northwesterly striking thrust fault (Figure 5). This section of the fault is referred to as the Homestead Valley "slip gap" because it bears a net right-slip deficiency relative to the 3 to 4 m of slip observed on the adjacent fault segments [Kanamori et al., 1992; Sieh et al., 1993; Spotila and Sieh, 1994; K.W. Hudnut and S.C. Larsen, Slip distribution in the 1992 Landers, California earthquake sequence determined from geodetic data, submitted to Journal of Geophysical Research, 1994]. We focused on the wedge-shaped area between the Johnson Valley and the Kickapoo faults primarily because the interferogram there shows a dense pattern of parallel fringes which contrasts markedly in density and orientation with the fringe patterns observed both west of the Johnson Valley fault and east of the Homestead Valley fault (Figure 5). Between the faults, the fringes are closely spaced and trend about N160°E, parallel to the local strike of the Johnson Valley and Homestead Valley faults, whereas, on the opposite sides of these two faults, the fringes are widely spaced and merge with the fault trace at a high angle.

Our first interpretation of this pattern was that the wedge-shaped block bounded by the Johnson Valley and the Kickapoo faults might have rotated as one would expect between right-stepping, overlapping, right-lateral fault segments [e.g., Nur et al., 1986]. However, Figure 3a and the simulation of rotating blocks about a vertical axis (Figure 4a) show that such rotations would produce fringes perpendicular to the satellite track (i.e., an azimuth of 100°E). The observed fringes, however, strike parallel to the local direction of the Johnson Valley and Homestead Valley faults, suggesting instead that the strike of these faults controls the deformation or displacement of this block. In the case of distributed, simple shear, the faults would impose the direction of shear, and, in the case of a tilted block, the azimuth of the rotation axis. We have shown in the previous section that in both of these cases the fringes would be parallel to the Johnson Valley and Homestead Valley faults. Deciding between these two hypotheses cannot be done using solely the information provided by the interferogram, which depicts only one component of the surface displacement field. However, the

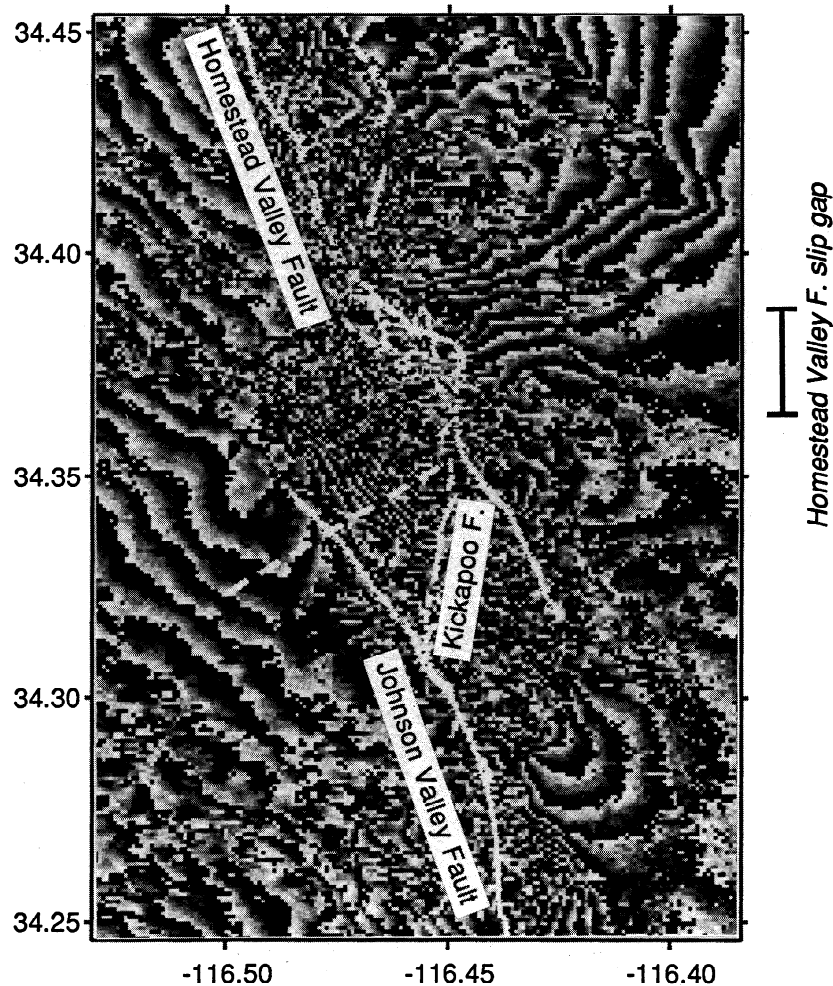


**Figure 5.** Detail of coseismic interferogram of Figure 1 in the area of the Johnson Valley, Kickapoo, Homestead Valley fault junction (see location in Figure 1). Surface rupture is from *Sieh et al.* [1993]. Dashed line indicates location of profile in Figure 7.

consistently equidistant, parallel fringes across an area of  $\sim 2 \times 5$  km implies a departure from an elastic behavior. In an elastic shear zone, the displacement gradient, and thus the density of the fringes, are expected to decrease gradually from the center to the edge of the shear zone. In the case of block tilting, the equidistant fringes imply a nearly rigid behavior. Furthermore, significant vertical offsets occurred along the block-bounding fault segments, supporting the tilted block hypothesis rather than distributed shear (which would not involve much vertical displacement).

Vertical offsets along the Johnson Valley fault [Sowers *et al.*, 1994] produced east-facing scarps north of the junction with the Kickapoo fault, and west-facing scarps south of the junction, suggesting differential vertical displacements of the northern block relative to the southern block. Vertical offsets along the Kickapoo fault, generally with west side up, and pronounced reverse displacement on the "slip gap" segment of the Homestead Valley fault, both indicate relative uplift of the block edge west of the northern reach of the Kickapoo fault. A down-to-the-southwest tilt of the block bounded by the Johnson Valley and the Kickapoo faults about an axis trending  $N20^\circ W$  would explain both the vertical displacements observed in the field and the dense fringe pattern observed in the interferogram.

Assuming that the block between the Johnson Valley and the Kickapoo faults has been tilted during the earthquake, it is possible to quantify the direction and amount of tilt from the interferogram. First, the tilt axis must be parallel to the local direction of fringes, i.e.,  $\sim N20^\circ W$ . Second, the variation of the phase within a cycle indicates that the displacement of the ground towards the satellite (uplift) increases with the distance northeast from the Johnson Valley fault. This relationship shows that the tilt is down towards the southwest. Third, the average distance between consecutive fringes along a 1.5-km-long profile in the zone of dense fringe pattern is  $d_f = 162 \pm 10$  m. This value and equation (2) constrain the tilt angle to  $t = 0.01^\circ \pm 0.0005^\circ$  ( $190 \pm 10$   $\mu\text{rad}$ ), assuming the satellite incidence angle to be constant at  $23^\circ$ . The uncertainty in these values reflects only the variations in length of profiles along which 10 fringes could be counted in the interferogram. It is important to note that any rigid translation of the block, superimposed to the tilt, would result in a uniform phase shift throughout the block area and would not affect the observed fringe spacing.

The direction and amount of tilt inferred from the interferogram appear to be generally consistent with the distribution of vertical offset observed along the Kickapoo fault and along the thrust segment of the Homestead Valley

fault. Figure 6 shows that vertical offsets measured along these faults [Sieh *et al.*, 1993; Hart *et al.*, 1993] tend to increase northeastward with the distance from the Johnson Valley fault, at least along the portion that we suggest has tilted. The apparent inconsistency of the offset distribution along the fault strike probably results from the left-stepping, en échelons geometry of the Kickapoo fault. In particular, the surface deformation gets distributed over a larger number of fractures in the north (approximately 3.2 km from the Johnson Valley fault, Figure 5) than it is in the south. Small vertical displacements are generally measured near the ends of any one individual échelon break, and larger offsets measured in their centers. Although more compelling field observations might better corroborate the interpretation based on the interferogram, the observed distribution of measured surface offsets certainly permits a down-to-the-west tilt of  $0.01^\circ$  of the block between the Kickapoo and the northern Johnson Valley faults.

Spotila and Sieh [1994] interpret the extensive secondary fissures observed west of the Homestead Valley thrust segment as evidence of distributed deformation in the volume of rocks adjacent to the fault. These observations are not inconsistent with our observation that the western half of the tilted block, i.e., the area where the interferogram depicts straight, equidistant fringes (Figure 5), behaved rigidly during the 1992 earthquake. Figure 6 shows that largest vertical offsets measured in the field are generally larger than predicted offsets using the tilted block model, suggesting that additional deformation may have taken place near the fault. Such additional deformation may also be responsible for the loss of coherence of the interferogram in the vicinity of the Kickapoo and Homestead Valley faults (Figure 5). Similarly, the block east of the Kickapoo fault appears incoherent in the interferogram and seems to have experienced extensive secondary faulting during the earthquake [Sowers *et al.*, 1994].

Analysis of the morphology of the Homestead valley [Sowers *et al.*, 1994] and paleoseismic studies [Rockwell *et al.*, 1993; Spotila and Sieh, 1994] show that these faults have been active during the Quaternary and may have previously

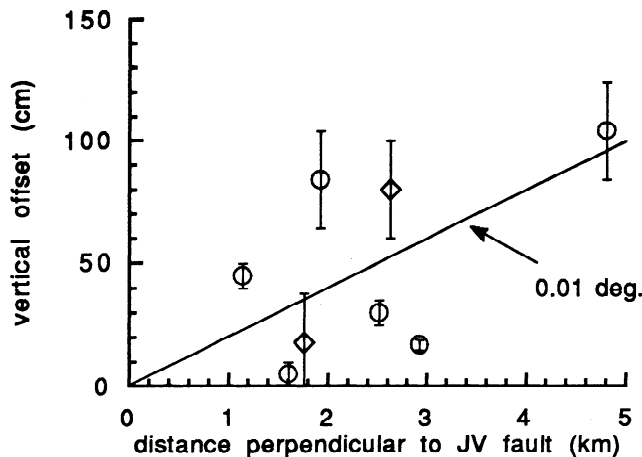


**Figure 6.** Variation of vertical offset measured along the Kickapoo and the southern Homestead Valley faults (west side up) as function of distance from Johnson Valley fault. Data are from Sieh *et al.* [1993] (circles) and Hart *et al.* [1993] (diamonds). Straight line indicates vertical offset predicted by tilted block model with tilt angle of  $0.01^\circ$  ( $190 \mu\text{rad}$ ).

ruptured in the manner of the 1992 earthquake. If the block between the Johnson Valley and the Kickapoo faults has been repeatedly tilted with past earthquakes, the cumulative effect of such tilts should be recorded in the topography. Figure 7a shows a topographic profile perpendicular to the Johnson Valley fault, and Figure 7b the elevation profile from which the average slope profile was subtracted. Although slopes of alluvial fans are generally concave up [e.g., Troeh, 1965], a break in the slope of profile in Figure 7b is clear and is consistent with a down-to-the-west tilt of the northeast block. Exponential curves fit to the upper (line AB) and lower (line CD) parts of the fan profile, respectively, intersect at an angle of  $0.15^\circ$ , about 15 times the coseismic tilt angle inferred above for the 1992 event. Geologic mapping and gravity measurements of the area indicate the existence of an east-facing subsurface bedrock escarpment associated with the northern Johnson Valley fault [Sowers *et al.*, 1994]. By contrast, the data do not indicate long-term, cumulative vertical displacement across the Kickapoo fault. These observations suggest that, if similar block tilting repeatedly occurred with earthquakes, it was associated with the subsidence of the western part of the block, against the Johnson Valley fault plane rather than with the uplift of its eastern side, as the 1992 east-facing scarps observed along the Kickapoo fault suggest.

**The Johnson Valley-Eureka Peak Surface Rupture Gap**

The surface fault ruptures along the Johnson Valley fault die out north of Yucca Valley and reappear south of the Pinto

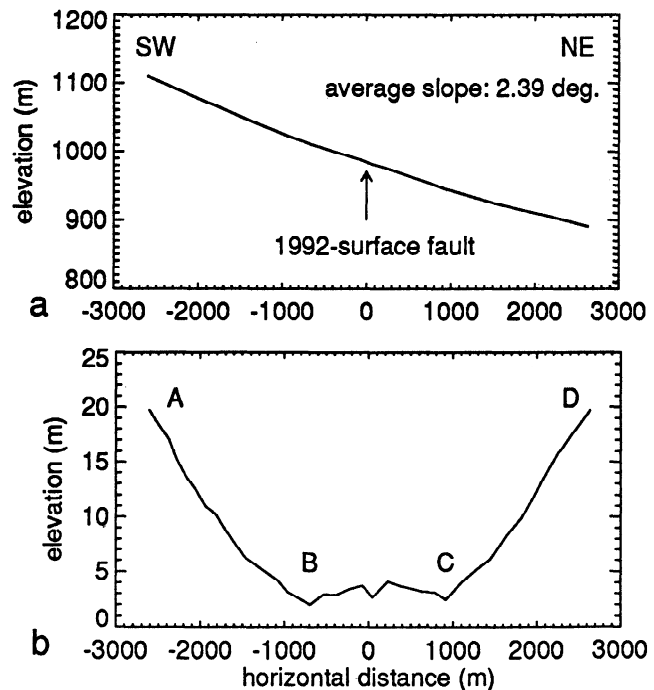


**Figure 7.** (a) Topographic profile perpendicular to the Johnson Valley fault (see location in Figure 5). Origin of horizontal axis is at the fault and values are positive towards the northeast. Vertical exaggeration is 7.7X. Average slope is  $2.39^\circ$ . Topographic data are from USGS 7.5 min. map. (b) Same profile as in Figure 7a with average slope  $2.39^\circ$  subtracted. Vertical exaggeration is 127X.

Mountain fault, along the Burnt Mountain and Eureka Peak faults [Sieh *et al.*, 1993; Hart *et al.*, 1993]. In this 6.5-km-long gap in surface breaks, the interferogram shows a pattern of dense fringes roughly parallel to the local direction of the southern Johnson Valley and Eureka Peak faults, suggesting that slip took place at depth on this segment (Figure 8). This interpretation is supported by the continuous distribution of aftershocks along this segment [Hauksson *et al.*, 1993]. A more convincing evidence of a continuous north-trending fault break comes from the seismic guided Love waves generated by aftershocks and trapped in the low-velocity fault zone [Li *et al.*, 1994]. These trapped waves reveal a ~180-m-wide low-velocity zone extending continuously through the intersection with the Pinto Mountain fault [Li *et al.*, 1994]. The surface expression of strike-slip displacement occurring on a buried fault would be a zone of distributed shear parallel to the fault direction. We have shown in the previous section that distributed shear results in dense fringes parallel to the shear direction (Figure 3c), similar to the pattern observed between the Johnson Valley fault and the Eureka Peak fault ruptures (Figure 8). The average distance between consecutive fringes measured along a 3.6-km-long profile, perpendicular to the shear direction is  $d_y=331$  m. With a shear direction of  $\delta=130^\circ$ , satellite track azimuth  $\alpha=10^\circ$ , radar wavelength  $\lambda=56.6$  mm and incidence angle  $\theta=23^\circ$ , equation (3) allows us to compute

the shear coefficient  $\gamma=2.9 \times 10^{-4}$  of the shear zone. Such a shear may be produced by a right-lateral displacement of 1 m, distributed over a 3.6-km-wide shear zone. Because the interferogram is incoherent east of the dense shear zone, several fringes are probably missing in this calculation. Therefore, the 1-m slip inferred above may represent a lower bound of the total displacement on the fault at depth.

There are no independent observations to test directly this inference and it is generally difficult to determine details of slip on blind fault breaks. Inversions of geodetic data imply 0.8 to 1.8 m of right-lateral slip at depth in the gap [e.g., Wald and Heaton, 1994; K.W. Hudnut and S.C. Larsen, submitted manuscript, 1994] (Figure 9). However, such inversions were neither posed so as to resolve details such as the locking depth in the surface break gap nor so that the distribution or amount of slip with depth be exactly determined. The SAR interferogram helps constrain these parameters. If the width of the intense shear zone is about twice the depth of the fault, then the top of the rupture plane must be about 1.5-2 km below the surface between the Johnson Valley and the Eureka Peak faults. We compute synthetic interferograms obtained by elastic dislocation modeling for three different fault depths in the surface rupture gap. The elastic model covers a 15 km by 15 km area centered on the surface break gap. The southern Johnson Valley fault,

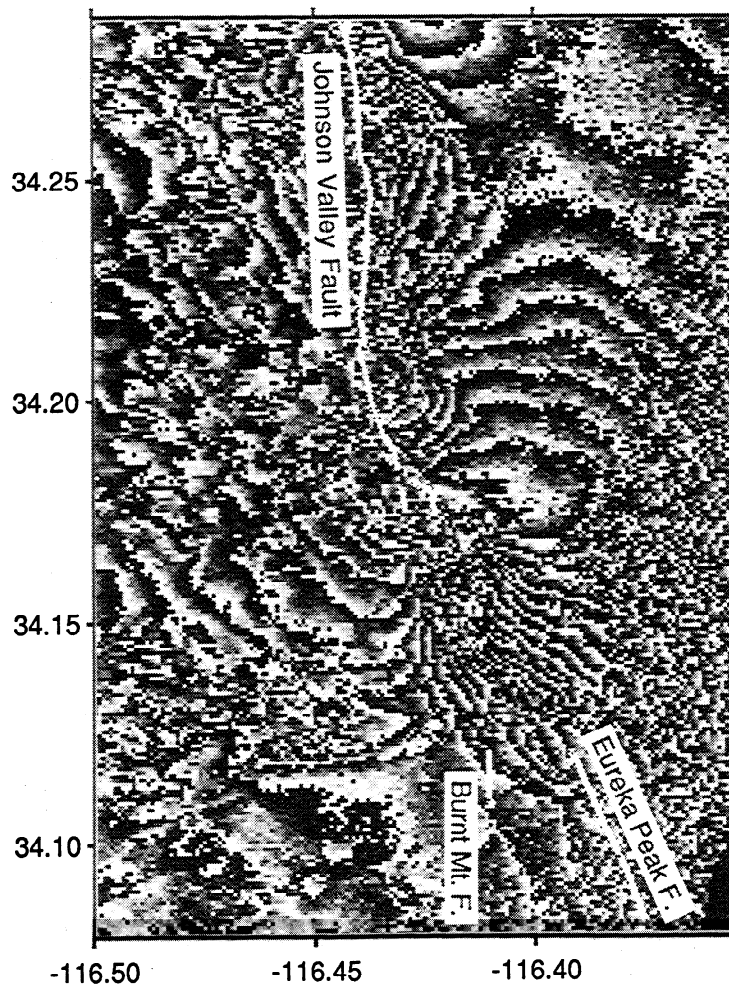


**Figure 8.** Detail of the coseismic interferogram of Figure 1 in area of surface rupture gap between Johnson Valley and Eureka Peak faults (see location in Figure 1). Fault traces from Sieh *et al.* [1993].

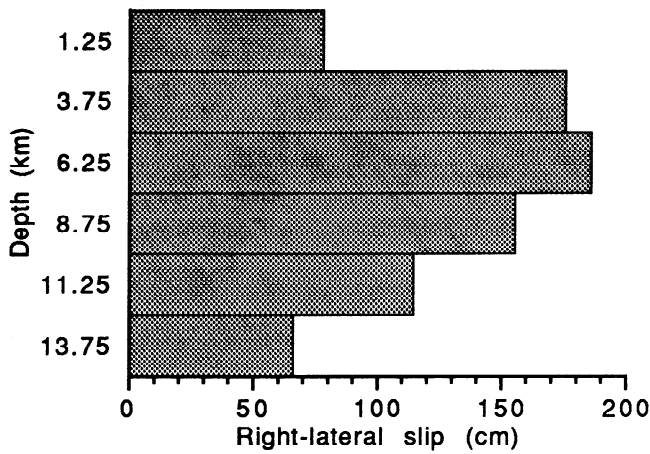


**Figure 9.** Distribution of slip at depth in the Johnson Valley, Eureka Peak faults surface rupture gap derived from inversion of geodetic data (K.W. Hudnut and S.C. Larsen, submitted manuscript, 1994).

the Eureka Peak fault, and the buried fault in the gap are modeled as three vertical planes. The distribution of slip at depth for the Johnson Valley and Eureka Peak faults is based on results of inversion of geodetic data (K.W. Hudnut and S.C. Larsen, submitted manuscript, 1994). Our results show that using the slip distribution of K.W. Hudnut and S.C. Larsen (submitted manuscript, 1994) (Figure 9) for the buried fault segment would not produce as many fringes in the gap as we observe in the SAR interferogram (Figure 8). This discrepancy may be explained by the fact that the geodetic model represents the entire rupture and may include compensation for

slip on other fault segments by lessening slip along this segment and that geodetic coverage was too sparse to resolve details that SAR can detect. The modeled interferograms shown in Figure 10a are computed using twice the amount of slip derived by K.W. Hudnut and S.C. Larsen (submitted manuscript, 1994) for each depth patch on that segment. The fault segment in the gap is locked above depths of 0.5, 1.5, and 3.0 km in the three modeled cases.

A quantitative comparison of the SAR interferogram with the models of Figure 10a can be done by measuring the fringe separation along a profile perpendicular to the fault in the middle of the gap (Figure 10b). The curves in Figure 10b correspond to the three models of Figure 10a. A shallow locking depth would produce dense fringes (small spacing) in the center of the shear zone, whereas more slip, deeper on the fault, would tend to distribute the deformation more evenly across the shear zone. The effect of varying the amount of slip for a given locking depth would be to change the average fringe spacing, and thus would come to shift the curves parallel to the ordinates axis. Figure 10b shows that the observed fringe pattern can be explained by doubling the distribution of slip at depth derived by K.W. Hudnut and S.C. Larsen (submitted manuscript, 1994) for the buried fault, with a locking depth of approximately 1.5-2 km.

**Discussion and Conclusion**

Both the analysis and implications of the SAR interferogram have brought new insights into displacement gradients in the vicinity of the Landers fault rupture. Because of the high sensitivity of the technique to components of ground displacements in the direction of the radar, extremely

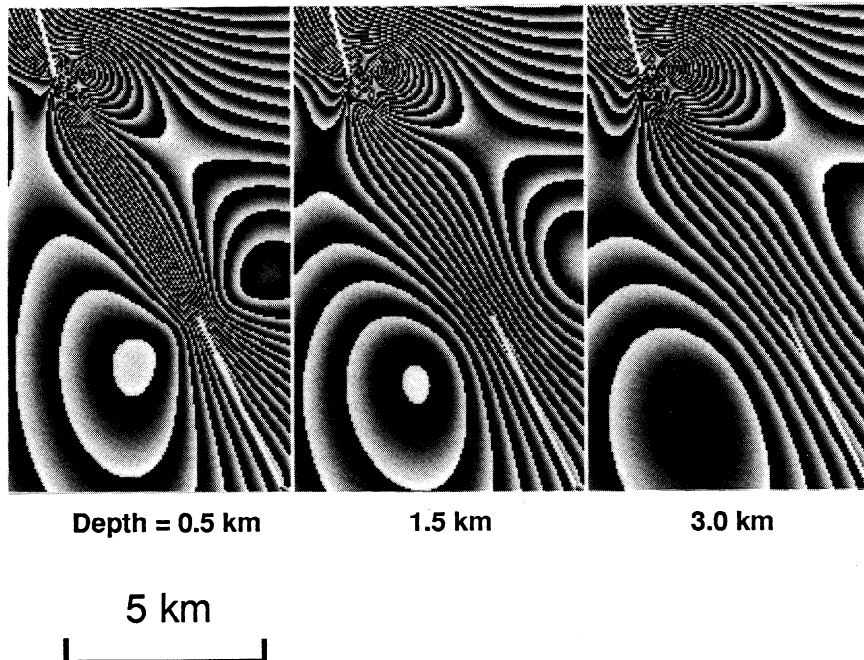


**Figure 10a.** Synthetic interferograms obtained by elastic dislocation modeling for three different locking depths in surface rupture gap between the Johnson Valley and Eureka Peak faults. Original model area extent is 15 km x 15 km. Figures depict smaller areas centered on zone of interest. Locking depth in gap is indicated. White lines are surface traces of Johnson Valley (top left) and Eureka Peak (bottom right) faults as modeled. Buried fault connecting these two faults at depth is not shown.

small gradients of the displacement field can be measured. For the same reason, large displacement gradients saturate the interferometric system, resulting in incoherent interferograms. In most sections of the fault, the Landers earthquake interferogram shows a zone of apparent decorrelation in the vicinity of the rupture. Two reasons can be advanced for the loss of coherence near the fault. First, some segments of the fault follow mountain ranges with rough topographic terrain reducing the level of correlation between the two SAR images [Zebker *et al.*, 1994a]. This problem could be partly overcome by using a pair of SAR images acquired from orbits closer together, thus reducing the sensitivity of the interferogram to topography [Li and Goldstein, 1990]. Second, the displacement gradient in those areas near the fault is sufficiently large to produce more than one phase cycle per image pixel. Given the pixel separation of 20 m in ground range for flat terrain in ERS-1 SAR images [European Space Agency, 1992], the threshold gradient above which the coherence is lost is around 1 per 1000. In cases where the noise in the data requires averaging over several SAR pixels, the above value is reduced by the averaging factor. The technique is thus not best adapted to studying natural processes involving high strain of the Earth's surface.

At the other end of the spectrum, extremely small displacements can be detected readily. The limit of detection varies, depending on the need to average the data for phase noise reduction and on the surface area involved with a consistent strain pattern. Given the limitations we discuss, we have shown that it is possible to map the displacement field resulting from an earthquake with a level of detail not attainable by other geodetic techniques. A convenient way of analyzing quantitatively local interferometric fringe patterns is to measure the local fringe direction and separation in regions where characteristic patterns can be recognized. The fringe direction informs us about the orientation of the local displacement gradient, and the fringe separation is a measure of its intensity. Forward modeling of simple deformation cases allows us to place constraints on the displacement gradient in two sections of the Landers 1992 rupture where coherent fringe patterns were observed. Between the northern

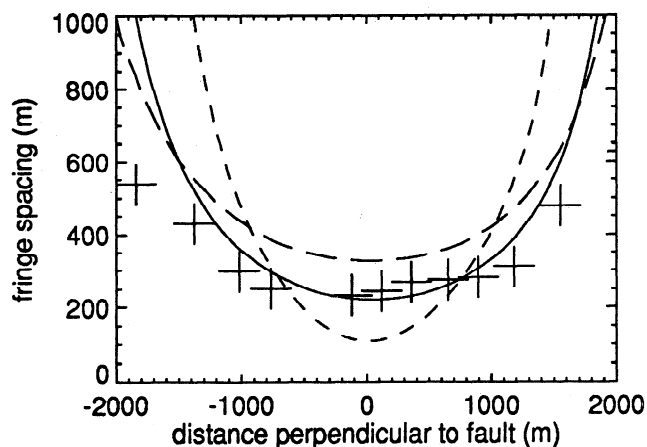


**Figure 10b.** Comparison of observed (crosses) and modeled (curves) fringe intervals along a profile perpendicular to the fault in middle of surface rupture gap. Curves correspond to models of Figure 10a with locking depth of 0.5 km (short dashes), 1.5 km (solid line) and 3 km (long dashes).

end of the Johnson Valley fault and the Kickapoo fault, the interferogram shows a dense pattern of parallel fringes consistent with a rigid-block tilt (down to the southwest) of the  $\sim 3 \times 5$  km crustal block bounded by these faults of about  $0.01^\circ$  ( $190 \mu\text{rad}$ ). In the surface rupture gap between the Johnson Valley and the Eureka Peak faults, the pattern of dense fringes can be explained by distributed shear produced by 1.2-3.8 m of slip on a buried segment of the fault, with slip occurring at depth greater than 1.5-2 km. Similar dense patterns of fringes are barely visible between the Homestead Valley and Emerson faults, but the level of noise in the interferogram in this area prevented us from clearly interpreting the ground displacement gradient there. We have shown that rigid-body rotations about a vertical axis would produce characteristic fringes perpendicular to the satellite track. We did not observe such patterns in the coherent part of the interferogram near the fault.

Besides the limitations we discuss, the technique of SAR interferometry provides a powerful way of investigating short-wavelength features of the surface displacement field, bringing new insights into earthquake rupture processes and fault segmentation.

**Acknowledgments.** We would like to thank the many geologists of the surface faulting mapping groups at Caltech, led by K. Sieh, and at USGS-Menlo Park, as well as T. Rockwell, S. Lindvall, J. Spotila, and J. Sowers for sharing their results in advance of publication. We also thank E. Ivins and A. Sylvester for comments on the early version of the manuscript. The paper benefited from the constructive reviews of P. Spudich, K. LaJoie, and K. Raney. The research described in this paper was carried out by the Jet Propulsion Laboratory under contract with NASA.

## References

- European Space Agency, ERS-1 System, 87 pp., ESA Publi. Div., ESTEC, Noordwijk, The Netherlands, 1992.
- Goldstein, R.M., H. Engelhardt, B. Kamb, and R.M. Frolich, Satellite radar interferometry for monitoring ice sheet motion: Application to an Antarctic ice stream, *Science*, 262, 1525-1530, 1993.
- Hart, E.W., W.A. Bryant, and J.A. Treiman, Surface faulting associated with the June 1992 Landers earthquake, California, *Calif. Geol.*, 46, 10-16, 1993.
- Hauksson, E., L.M. Jones, K. Hutton, and D. Eberhart-Phillips, The 1992, Landers earthquake sequence: Seismological observations, *J. Geophys. Res.*, 98, 19,835-19,858, 1993.
- Johnson, A.M., R.W. Fleming, and K.M. Cruikshank, Broad belts of shear zones as the common form of surface rupture produced by the 28 June 1992 Landers, California, earthquake, *US Geol. Surv. open file rep.*, 93-348, 1993.
- Kanamori, H., H.K. Thio, D. Dreger, E. Hauksson, and T. Heaton, Initial investigation of the Landers California earthquake of 28 June 1992 using Terrascope, *Geophys. Res. Lett.*, 19 (22), 2267-2270, 1992.
- Li, F., and R.M. Goldstein, Studies of multi-baseline spaceborne interferometric synthetic aperture radars, *IEEE Trans. Geosci. Remote Sensing*, 28, 88-97, 1990.
- Li, Y.-G., K. Aki, D. Adams, A. Hasemi, and W. H. K. Lee, Seismic guided waves trapped in the fault zone of the Landers, California, earthquake of 1992, *J. Geophys. Res.*, 99, 11,705-11,722, 1994.
- Massonnet, D., M. Rossi, C. Carmona, F. Adragna, G. Peltzer, K. Feigl, and T. Rabaute, The displacement field of the Landers earthquake mapped by radar interferometry, *Nature*, 364 (6433), 138-142, 1993.
- Nur, A., H. Ron, and O. Scotti, Fault mechanics and the kinematics of block rotations, *Geology*, 14, 746-749, 1986.
- Rockwell, T.K., D.P. Schwartz, K. Sieh, C. Rubin, S. Lindvall, M.

- Herzberg, D. Padgett, and T. Fumal, Initial paleoseismic studies following the Landers earthquake: Implication for fault segmentation and earthquake clustering, *Eos Trans. AGU*, 74 (43), fall meeting suppl., 67, 1993.
- Sieh, K., L. Jones, E. Haukson, K. Hudnut, D. Eberhart-Phillips, T. Heaton, S. Hough, K. Hutton, H. Kanamori, A. Lilje, S. Lindvall, S. McGill, J. Mori, C. Rubin, J. Spotila, J. Stock, Hong Kie Thio, J. Treiman, B. Wernicke, and J. Zachariassen, Near-field investigations of the Landers earthquake sequence, April to July 1992, *Science*, 260, 171-176, 1993.
- Sowers, J.M., J.R. Unruh, W.R. Lettis, and T.D. Rubin, Relationship of the Kickapoo fault to the Johnson Valley and Homestead Valley faults, San Bernardino County, California, *Bull. Seismol. Soc. Am.*, 84 (3), 528-536, 1994.
- Spotila, J. A., and K. Sieh, Geologic investigation of a "slip gap" in the surficial ruptures of the 1992 Landers earthquake, southern California, *J. Geophys. Res.*, in press, 1994.
- Troch, F.R., Landform equations fitted to contour maps, *Am. J. Sci.*, 263, 616-627, 1965.
- Wald, D., and T. Heaton, Spatial and temporal distribution of slip for the 1992 Landers, California, earthquake, *Seismol. Soc. Am. Bull.*, 84 (3), 668-691, 1994.
- Zebker, H.A., and J. Villasenor, Decorrelation in interferometric radar echoes, *IEEE Trans. Geosci. Remote. Sens.*, 30, (5), 950-959, 1992.
- Zebker, H.A., C. Werner, P. Rosen, and S. Hensley, Accuracy of topographic maps derived from ERS-1 interferometric radar, *IEEE Trans. Geosci. Remote. Sens.*, 32 (4), 832-836, 1994a.
- Zebker, H. A., P. Rosen, R.M. Goldstein, A. Gabriel, and C.L. Werner, On the derivation of coseismic displacement fields using differential radar interferometry: The Landers earthquake, *J. Geophys. Res.*, in press, 1994b.
- 
- K.L. Feigl, CNRS, UPR 234, Observatoire Midi-Pyrénées, Toulouse, France.
- K.W. Hudnut, U.S. Geological Survey, Pasadena, CA 91125.
- G. Peltzer, Jet Propulsion Laboratory, California Institute of Technology, 4800 Oak Grove Drive, Pasadena, CA 91109.

(Received February 28, 1994; revised June 22, 1994; accepted July 18, 1994.)